CERN – EUROPEAN ORGANIZATION FOR NUCLEAR RESEARCH

CLIC – Note – 1139

# STRAY MAGNETIC FIELD TOLERANCES FOR THE 380 GEV CLIC DESIGN

Chetan Gohil[1], Daniel Schulte[2], Philip N. Burrows[1]

[1]JAI, University of Oxford, Oxford, United Kingdom
[2]CERN, Geneva, Switzerland

CERN-ACC-2018-0052
19/11/2018

**Abstract**

The amplitude of external dynamic magnetic fields that can be tolerated by the 380 GeV CLIC design are presented along with the effect of different correction techniques. Different spatial distributions for the magnetic fields are considered. This includes a sinusoidal spatial dependence, a constant valued magnetic field across the entire accelerator and a random variation of the magnetic field from point to point.

Geneva, Switzerland
19 November 2018

# Stray Magnetic Field Tolerances for the 380 GeV CLIC Design

C. Gohil[1], D. Schulte[2], and P.N. Burrows[1]

[1]JAI, University of Oxford, Oxford, OX1 3PA, United Kingdom
[2]CERN, Geneva, Switzerland

(November 19, 2018)

**Abstract**

The amplitude of external dynamic magnetic fields that can be tolerated by the 380 GeV CLIC design are presented along with the effect of different correction techniques. Different spatial distributions for the magnetic fields are considered. This includes a sinusoidal spatial dependence, a constant valued magnetic field across the entire accelerator and a random variation of the magnetic field from point to point.

## 1 Introduction

This paper concerns external (referred to as stray) magnetic fields, of which only dynamic magnetic fields are discussed. The temporal variation of the stray field is assumed to be slow enough that the same amplitude is seen across a single bunch train (or pulse). It is also assumed that the temporal variation is slow enough that the stray field appears static to a pulse as it travels through the accelerator. However, the temporal variation does lead to a pulse to pulse variation of the stray field. Such a scenario is valid for frequencies up to a few MHz. The stray field also has a spatial variation, which can be particularly detrimental if it is in resonance with the betatron motion of the beam. Three different spatial variations are considered: those with a sinusoidal variation, referred to as sinusoidal stray fields; those which have a constant value across the entire accelerator, referred to as coherent stray fields, and those which vary randomly with position along the beamline, referred to as Gaussian stray fields.

Previous studies of sinusoidal stray fields for the 3 TeV CLIC design [1, 2] have shown sensitivities to nT amplitudes and other studies of the 380 GeV design [3] show a similar level of sensitivity. Further simulations of sinusoidal stray magnetic fields in the 380 GeV CLIC design are presented with the effect of different mitigation techniques.

Simulations were performed with the particle tracking code PLACET [4]. To represent the stray field a grid of zero length dipole elements were inserted into the lattice with a spacing of 1 m. The strength of each dipole was set to apply the integrated kick from the stray field over the space between dipoles. The dipoles were used to kick the beam in the vertical direction to simulate the effect of a stray field orientated in the horizontal plane. The kick from a stray field is related to its amplitude by

$$\delta\ [\mu\text{rad}] = \frac{c \cdot \Delta s\ [\text{m}] \cdot B\ [\text{nT}]}{E\ [\text{GeV}]} \times 10^{-12}, \tag{1}$$

where $\delta$ is the dipole kick, $c$ is the speed of light, $\Delta s$ is the distance between kicks, $B$ is the amplitude of the stray field and $E$ is the energy of the beam.

# 2 Tolerances

A stray field can lead to luminosity loss in two way: by inducing an offset between the colliding beams at the interaction point (IP) or via emittance growth. The luminosity of two bunches colliding with an offset is given by

$$\mathcal{L} = \frac{N_1 N_2 f N_b}{4\pi\sigma_{x,0}\sigma_{y,0}}\mathcal{H}_D \cdot \exp\left(-\frac{y^2}{4\sigma_{y,0}^2}\right), \tag{2}$$

where $N_1$ ($N_2$) is the number of particles in the first (second) bunch, $f$ is the repetition rate, $N_b$ is the number of bunches, $\sigma_{x,0}$ ($\sigma_{y,0}$) is the horizontal (vertical) beam size, $\mathcal{H}_D$ is a disruption parameter due to the electromagnetic interaction of the colliding bunches and $y$ is a vertical offset between them. However, this is equivalent to a collision of two beams with no offset, but with an increased beam size given by

$$\sigma_{y,\text{eff}} = \sigma_{y,0}\exp\left(\frac{y^2}{4\sigma_{y,0}^2}\right). \tag{3}$$

This increase in beam size can be written in terms of emittance as

$$\epsilon_{y,\text{eff}}(y) = \epsilon_{y,0}\exp\left(\frac{y^2}{2\sigma_{y,0}^2}\right) \approx \epsilon_{y,0}\left(1+\frac{y^2}{2\sigma_{y,0}^2}\right) \approx \epsilon_{y,0} + \Delta\epsilon_{y,\text{eff}}(y), \tag{4}$$

where $\epsilon_{y,0}$ is the ideal vertical emittance and $\Delta\epsilon_{y,\text{eff}}(y) = y^2/(2\sigma_{y,0}^2)$ is an effective emittance growth due to the offset. Similarly, an angle can be written as an effective emittance growth as

$$\epsilon_{y,\text{eff}}(y') \approx \epsilon_{y,0}\left(1+\frac{y'^2}{2\sigma_{y',0}^2}\right) \approx \epsilon_{y,0} + \Delta\epsilon_{y,\text{eff}}(y'), \tag{5}$$

where $\Delta\epsilon_{y,\text{eff}}(y') = y'^2/(2\sigma_{y',0}^2)$.

To account for the effect of an offset and angle at the end of a section Eqs. (4) and (5) are used to give a total effective emittance growth due to a stray field,

$$\Delta\epsilon_{y,\text{eff}} = (\epsilon_{y,\text{sim}} - \epsilon_{y,0}) + \frac{y_{\text{sim}}^2}{2\sigma_y^2} + \frac{y_{\text{sim}}'^2}{2\sigma_{y'}^2}, \tag{6}$$

where $\epsilon_{y,\text{sim}}$ is the emittance, $y_{\text{sim}}$ is the offset and $y'_{\text{sim}}$ is the angle given by the PLACET simulations.

A 2 % luminosity loss budget is allocated for the effects of stray magnetic fields in the 380 GeV CLIC design. This can be written as an equivalent emittance growth using

$$\mathcal{L} \propto \frac{1}{\sqrt{\epsilon_y}} \implies \frac{\mathcal{L}_0 + \Delta\mathcal{L}}{\mathcal{L}_0} = \sqrt{\frac{\epsilon_{y,0}}{\epsilon_{y,0}+\Delta\epsilon_y}} \implies \Delta\epsilon_y \approx -2\epsilon_{y,0}\frac{\Delta\mathcal{L}}{\mathcal{L}_0}, \tag{7}$$

where $\mathcal{L}_0$ is the ideal luminosity, $\Delta\mathcal{L}$ is a luminosity loss, $\epsilon_{y,0}$ is the ideal vertical emittance and $\Delta\epsilon_y$ is a vertical emittance growth. Using the nominal value of $\epsilon_{y,0} = 30$ nm in Eq. (7), a vertical emittance growth budget of $\Delta\epsilon_y = 1.2$ nm is obtained.

Tolerances of stray fields were calculated as the amplitude that corresponds to a 1.2 nm emittance growth at the end of a section. The emittance growth due to a stray field scales with the amplitude as

$$\Delta\epsilon_y \propto B^2. \tag{8}$$

Simulations were performed with amplitudes that result in an emittance growth ($\Delta\epsilon_{y,\,\mathrm{sim}}$) a few factors of the budget ($\Delta\epsilon_y \lesssim \Delta\epsilon_{y,\,\mathrm{sim}} \lesssim 3 \cdot \Delta\epsilon_y$). The amplitude used in the simulation is then rescaled with Eq. (8) to calculate the tolerance.

# 3 Sinusoidal Stray Fields

## 3.1 Ring to Main Linac Long Transfer Line

The tolerance for a sinusoidal stray field in the long transfer line in the Ring to Main Linac (RTML) is shown in Fig. 1. A sine function was used to generate the stray field with its origin placed at the start of the transfer line.

The sensitivity to stray fields in the the RTML transfer line is due to the long drifts and relatively weak focusing from the quadrupoles in the line. The minimum tolerance of 0.1 nT corresponds to the stray field wavelength approaching the betatron wavelength of the lattice.

Whether or not an offset or angle is present at the end of a section depends on the wavelength of the stray field. In some case, the kicks from the stray field cancel such that there is no final offset or angle. This leads to the periodic structure that is present in the tolerance with no TA correction, where increasing the wavelength results in a larger offset, leading to a tighter tolerance up until a point where increasing the wavelength then acts to reduce the final offset, loosening the tolerance.

The RTML contains a turn-around (TA) loop, which provides the possibility of adding a feed-forward mechanism to correct the trajectory of the beam before it enters the ML. Such a scheme would measure the offset of the beam near the start of the TA loop at two locations, which have a phase advance of 90° between them. This ables both the offset and angle of the beam at the end of the TA loop to be fully corrected. The tolerance with a feed-forward mechanism, shown in Fig. 1, indicates that the tolerance can be increased by two orders of magnitude with a perfect trajectory correction applied in the TA.

## 3.2 Main Linac and Beam Delivery System

The Main Linac (ML) and Beam Delivery System (BDS) were integrated into a single simulation. Two different BDS designs, which differ in the drift length ($L^*$) between the final quadrupole and IP, were simulated. Fig. 3 shows the tolerance for sinusoidal stray fields in the ML and BDS. The origin of the sinusoidal function used to generate the stray fields was placed at the IP. Two types of stray fields have been considered, those which are symmetric about the IP (Cosine) and those which are anti-symmetric about the IP (Sine). Sine-like stray fields introduce an offset at the IP, which is not present for cosine-like stray fields, generally leading to tighter tolerances.

Depending on the location of a kick, the effect it can have depends on the beta function, betatron phase and the energy of the beam at that location. A sensitivity function is defined as the final offset due to a single kick divided by the amplitude of the kick. Placing the integrated kick from a stray field at a single location, the sensitivity of the BDS, shown in Fig. 2, is found. The most sensitive locations are those in which a large

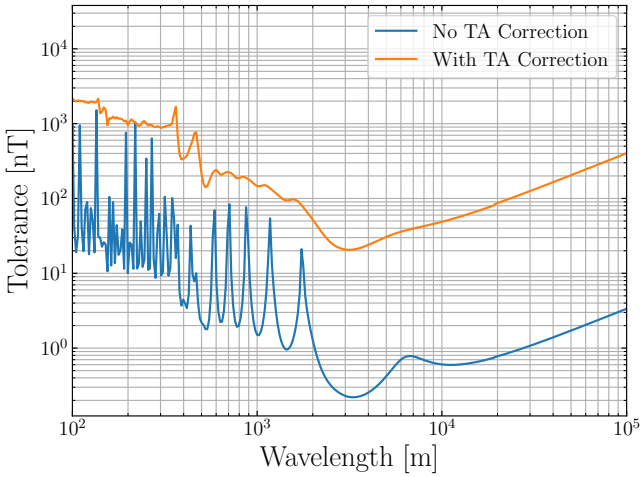


Figure 1: Tolerance for a 1.2 nm emittance growth in the RTML long transfer line, with and without a trajectory correction from a feed-forward mechanism in the turn-around (TA) loop.

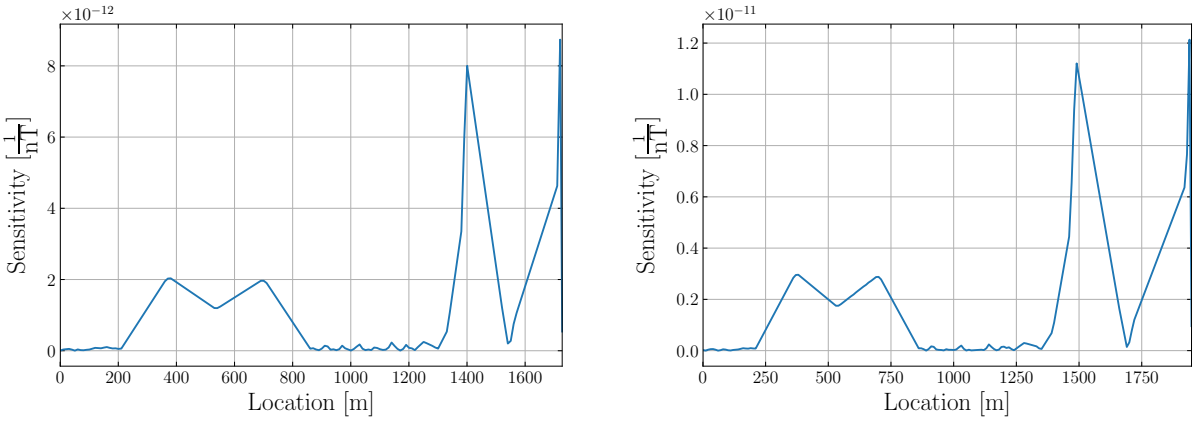


(a) $L^* = 4.3$ m. (b) $L^* = 6$ m.

Figure 2: Point sensitivity function of two BDS designs.

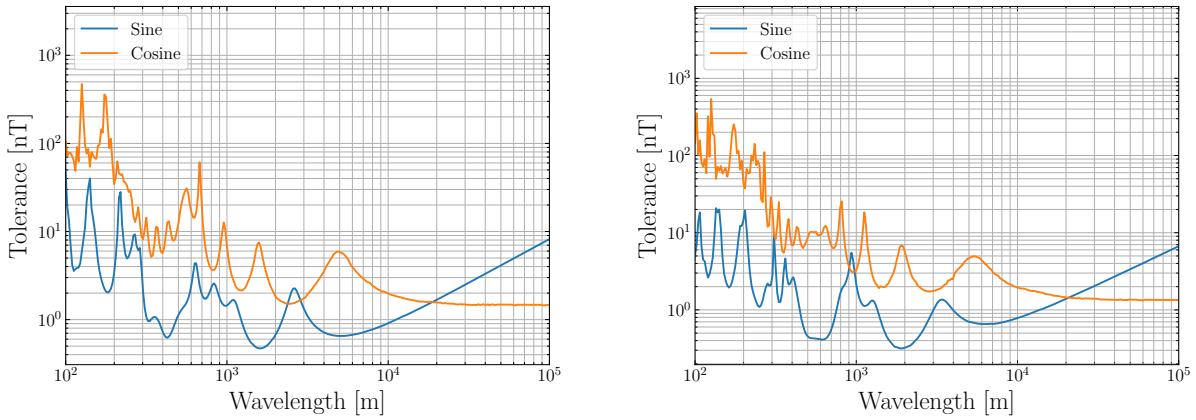


(a) $L^* = 4.3$ m. (b) $L^* = 6$ m.

Figure 3: Tolerance for a 1.2 nm emittance growth in the ML and BDS.

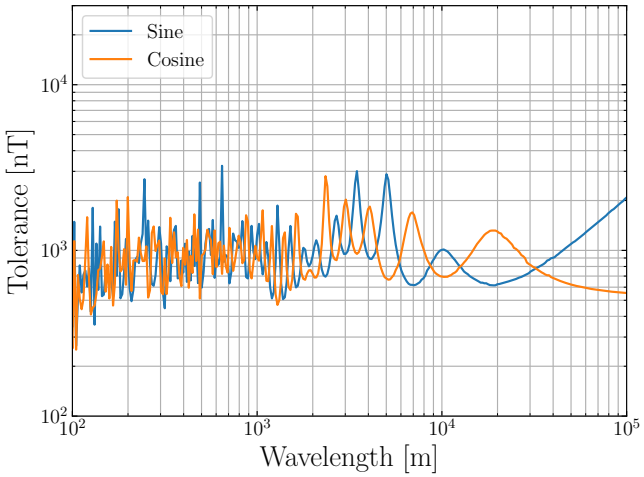


Figure 4: Tolerance for a 1.2 nm emittance growth in the ML and ($L^* = 6$ m) BDS with a perfect shield surrounding the entire BDS beamline.

beta function exists, i.e. in the collimation section and bends before the final focus. Comparing the wavelengths that exhibit the tightest tolerances with the spatial lengths of the sensitive regions of the BDS, it is clear that the tight tolerances in the BDS arise from cases where the stray field is at a maxima in the sensitive regions.

The minimum tolerance observed in Fig. 3 is approximately 0.1 nT for sine-like stray fields and a tolerance of approximately 1 nT emerges for long wavelength, cosine-like stray fields.

The effect of surrounding the BDS with a perfect magnetic shield is shown in Fig. 4. This demonstrates that the ML is the most robust section of the CLIC with respect to stray fields with tolerances on the order of $\mu$T. There will also be an additional benefit in the ML of magnetic shielding provided by the copper walls that form each cavity, suggesting that an effective mitigation strategy can be obtained by targeting just the RTML transfer line and BDS.

It may be possible to devise an effective strategy to mitigate the effects of stray fields by shielding parts of the BDS opposed to the entire BDS beamline. Fig. 5 shows the tolerance can be increased by an order of magnitude by surrounding just the collimation section and bends before the final focus with a perfect magnetic shield.

The effect of a perfect feedback system that completely removed the offset at the IP is shown in Fig. 6. The tolerance can be increased by an orders of magnitude with the IP feedback system. The IP feedback system is ineffective for cosine-like stray fields. This is because cosine-like stray fields kick the electron and positron beams in the same direction, ensuring there is no offset at the IP. Therefore, no benefit is obtained with an IP feedback system for cosine-like stray fields.

## 3.3 Stray Field Correctors

A mitigation strategy under consideration is the addition of stray field correctors that would be placed along the beamline to actively compensate the stray fields directly. An active corrector requires an additional sensor to measure the stray field to be compensated. Two studies have been performed investigating the effect using sensors of different lengths with the correctors.

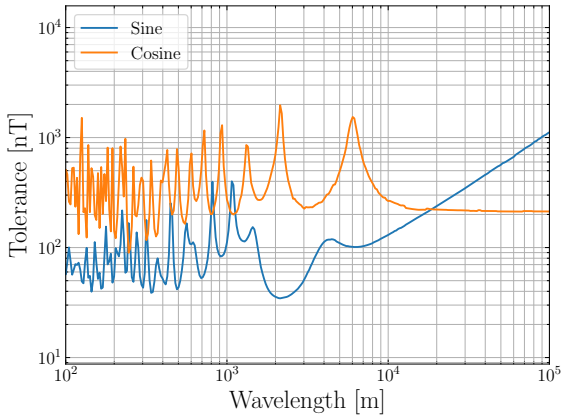


(a) $L^* = 4.3$ m.

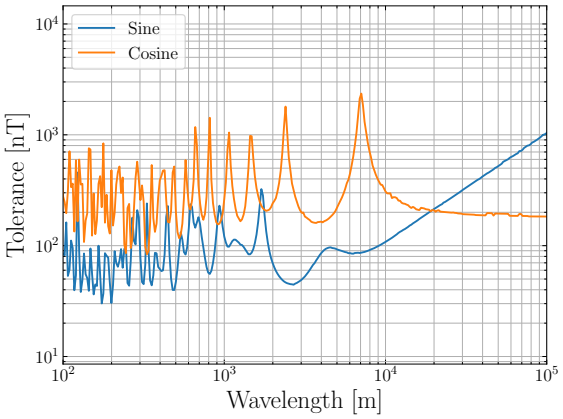


(b) $L^* = 6$ m.

Figure 5: Tolerance for a 1.2 nm emittance growth in the ML and BDS with a perfect shield surrounding the BDS collimation section and bends before the final focus.

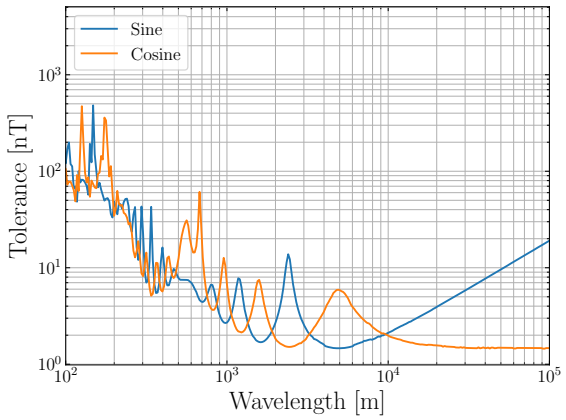


(a) $L^* = 4.3$ m.

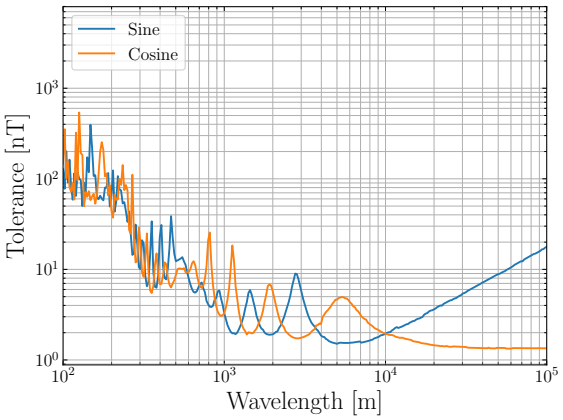


(b) $L^* = 6$ m.

Figure 6: Tolerance for a 1.2 nm emittance growth in the ML and BDS with a perfect IP feedback system.

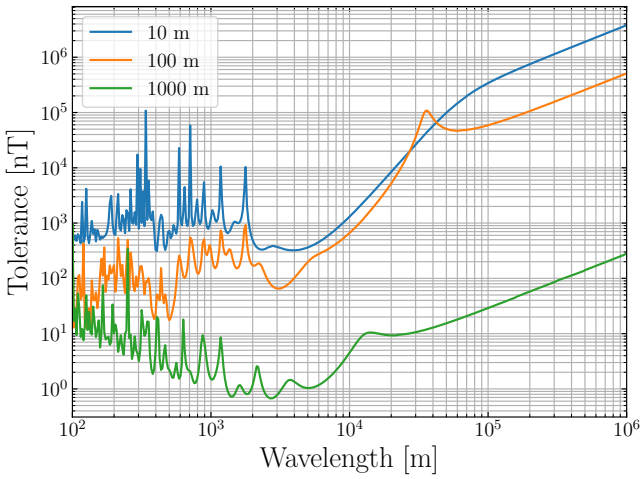


Figure 7: Tolerance for a 1.2 nm emittance growth in the RTML long transfer line with a series of correctors of a particular length placed along the beamline with sensors of the same length. No correction is applied in the TA.

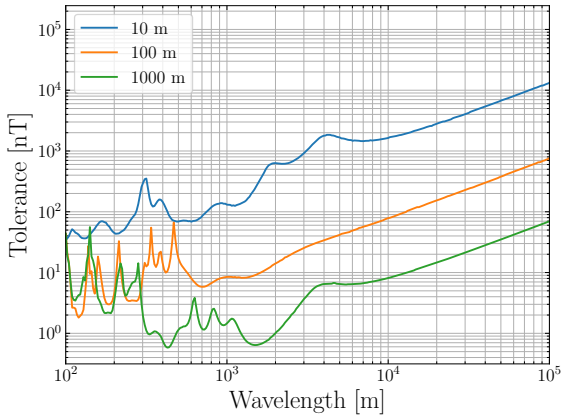


(a) $L^* = 4.3$ m. sine-like.

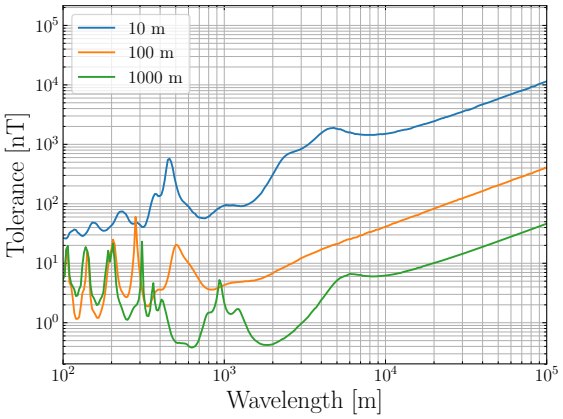


(b) $L^* = 6$ m, sine-like.

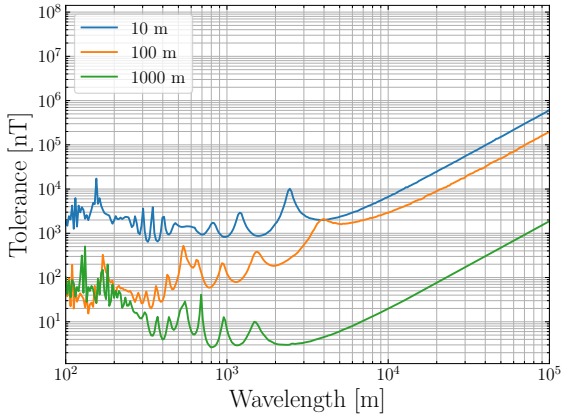


(c) $L^* = 4.3$ m, cosine-like.

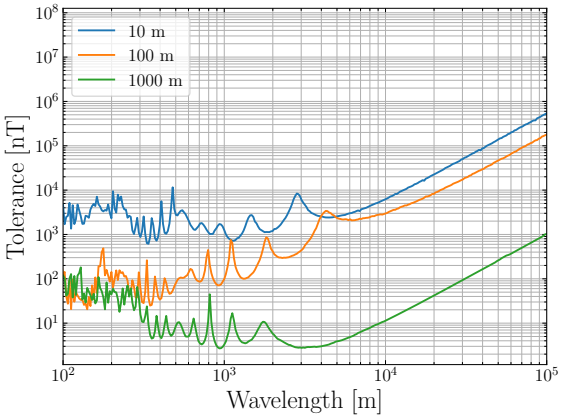


(d) $L^* = 6$ m, cosine-like.

Figure 8: Tolerance for a 1.2 nm emittance growth in the ML and BDS with a series of correctors of a particular length placed along the beamline with sensors of the same length.

The first study assumes the length of the sensor is the same as the corrector. Three different sensor/corrector lengths were considered: 10 m, 100 m and 1000 m. The sensors and correctors were placed consecutively along the entire beamline. The correction applied by each corrector was the average stray field measured across the length of the sensor.

Fig. 7 shows the tolerance with a series of correctors in the RTML transfer line. Sensors that measure the stray field over 1000 m would be ineffective as mitigation. This is due to the small wavelength stray fields being averaged over. Measurements over lengths of 100 m begin to correct the stray field more effectively and can remove the sensitivity to the betatron wavelength in the transfer line.

Fig. 8 shows the tolerance with a series of correctors with sensors of the same length in the ML and BDS. The addition of the correctors removes the constant tolerance that emerged for long wavelength, cosine-like stray fields. Sensors that measure over a length of 1000 m are ineffective in the ML and BDS.

Another study performed was the effectiveness of using a number of point-like sensors that measure the stray field at one location and use this value to apply a correction to a section of the beamline.

Fig. 9 shows the tolerance with a series of corrections of varying length, with a point-like sensor placed at the centre of the region in which the corrector acts. The point-like sensors appear to be slightly more effective at increasing the tolerance compared to the

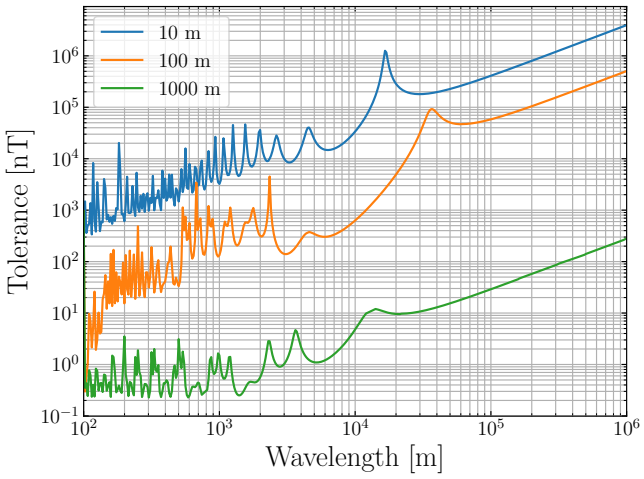


Figure 9: Tolerance for a 1.2 nm emittance growth in the RTML long transfer line with a series of correctors of a particular length placed along the beamline with point-like sensors place at the centre. No correction is applied in the TA.

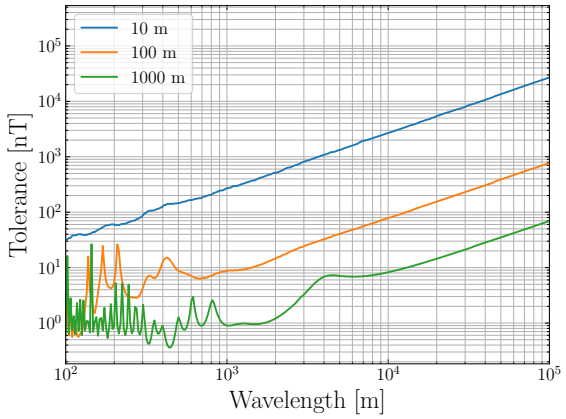


(a) $L^* = 4.3$ m. sine-like.

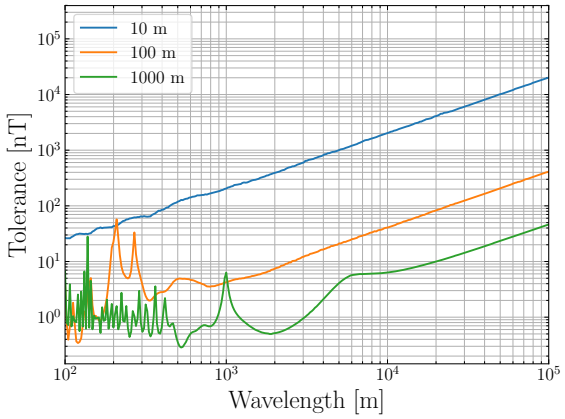


(b) $L^* = 6$ m, sine-like.

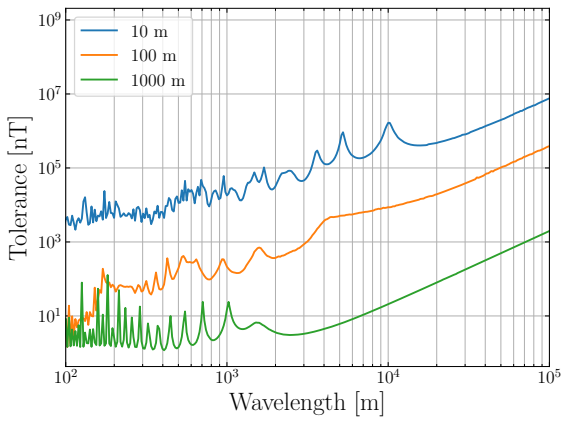


(c) $L^* = 4.3$ m, cosine-like.

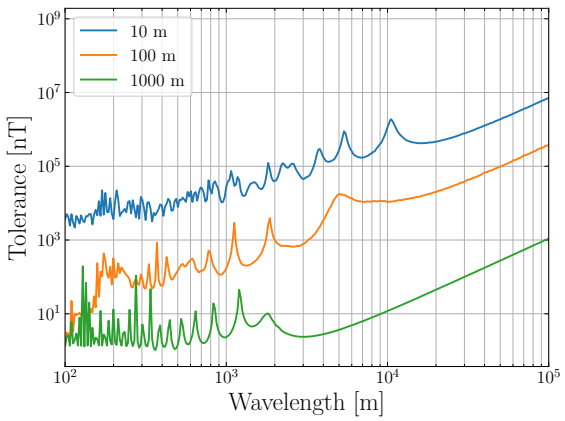


(d) $L^* = 6$ m, cosine-like.

Figure 10: Tolerance for a 1.2 nm emittance growth in the ML and BDS with a series of correctors of a particular length placed along the beamline with a zero length sensor placed at the centre of each corrector.

| Section(s) | Tolerance (nT) |
|---|---|
| RTML Transfer Line | 27 |
| ML | 540 |
| ML and BDS ($L^* = 4.3$ m) | 1.5 |
| ML and BDS ($L^* = 6$ m) | 1.3 |

Table 1: Tolerance for a 1.2 nm emittance growth from a coherent stray field in different sections of CLIC.

| Section(s) | Tolerance (nT) |
|---|---|
| RTML Transfer Line | 10 |
| ML and BDS ($L^* = 4.3$ m) | 6.3 |
| ML and BDS ($L^* = 6$ m) | 4.9 |

Table 2: Root-mean-square tolerances that corresponds to a 1.2 nm emittance growth from a Gaussian stray field in different sections of CLIC.

sensors that span the full length of the correctors.

# 4 Coherent Stray Fields

The effect of a constant valued (coherent) stray field across an entire section was also simulated. The tolerances for each section are shown in Tab. 1. The tolerance for long wavelength sinusoidal stray fields tends to the tolerance for coherent stray fields as expected.

Coherent stray fields are symmetric about the IP. This means that any offset due to a stray field will be mirrored by the colliding beams, such that there is no relative offset at the IP. Therefore, tolerances of coherent stray fields are from the secondary effect of the stray field to cause emittance growth.

# 5 Gaussian Stray Fields

Here, the stray field kick applied by each dipole was sampled from a Gaussian distribution. This represents a scenario after correction, where each point been left with some residual stray field from the noise in the corrector. Such a stray field represents a white noise that cannot be corrected.

Using a Gaussian distribution of mean zero and standard deviation 1 nT, each section was simulated 100 times and the emittance growth was averages. From this the tolerances shown in Tab. 2 were found.

# References


[1] J. Snuverink *et al.*, "Impact of Dynamic Magnetic Fields on the CLIC Main Beam", IPAC'10, Kyoto, Japan, May 2010.

[2] E. Marin, D. Schulte, B. Heilig, and J. Pfingstner, "Impact of Dynamical Stray Fields on CLIC", IPAC'17, Copenhagen, Denmark, May 2017.

[3] C. Gohil, P.N. Burrows, E. Marin, D. Schulte, and M. Buzio, "Measurements and Impact of Stray Fields on the 380 GeV Design of CLIC", IPAC'18, Copenhagen, Denmark, May 2017.

[4] A. Latina *et al.*, "Recent Improvements of the Tracking Code PLACET", EPAC'08, Genoa, Italy, June 2008.